Appl Biochem Biotechnol
DOI 10.1007/s12010-014-1019-7

Horseradish Peroxidase Enzyme Immobilized Graphene Quantum Dots as Electrochemical Biosensors

A. Muthurasu · V. Ganesh

Received: 13 January 2014 / Accepted: 19 June 2014

Abstract Green colour emitting graphene quantum dots (GQDs) are prepared by a simple acid reflux reaction of graphene oxide (GO) produced using a modified Hummer's method. Structural and morphological characterizations of such GQDs are performed using spectroscopic (FTIR, UV–vis and photoluminescence) and microscopic (transmission electron microscopy) techniques. These studies reveal the formation of stable, uniform spherical particles of GQDs which emit a green colour and possess surface functional moieties such as epoxide, hydroxyl (−OH) and carboxyl (−COOH) groups. Further, the possibility of immobilizing biomolecules on GQDs using these surface active functional groups is explored. As an example, an enzyme namely *horseradish peroxidase* (HRP) is shown to be anchored on these GQDs using a coupling reaction between an acid and amine leading to the formation of a peptide amide bond. Enzymatic activity of HRP is investigated by simply drop-casting HRP-immobilized GQDs onto a glassy carbon electrode. Electrochemical studies clearly reveal the formation of a well-defined redox peak and the dependence of redox peak current on scan rate suggests that the HRP enzyme is anchored onto the electrode, surface confined and exhibits a direct electron transfer process that is predominantly controlled by a diffusion process. These HRP-functionalized GQDs are used as a sensing platform for hydrogen peroxide detection. This particular electrochemical biosensor shows the sensitivity values of 0.905 and 7.057 μA/mM and detection limits of ~530 nM and 2.16 μM along with a fast response time of ~2–3 s.

Keywords Biosensors · Electrochemistry · Enzymes · Fluorescence · Graphene quantum dots · *Horseradish peroxidase* · Kinetic parameters

Introduction

Graphene quantum dots (GQDs) have become a major attraction in the recent years owing to their unique and interesting optical, electrical and chemical properties such as fluorescence, layered arrangement, high storage capability, the availability of surface functional groups, etc.

A. Muthurasu · V. Ganesh (✉)
Electrodics and Electrocatalysis (EEC) Division, CSIR–Central Electrochemical Research Institute (CSIR–CECRI), Karaikudi 630006 Tamilnadu, India
e-mail: vganesh@cecri.res.in

V. Ganesh
e-mail: ganelectro@gmail.com

Published online: 02 July 2014

[1–3]. GQDs have been applied in various fields including bio-imaging [4–13], photovoltaics [14], controlled drug delivery [15, 16], energy conversion—storage devices and sensor (both chemical and biological) applications [17, 18]. Depending upon the synthetic methodology employed for the preparation of GQDs, it is possible to produce GQDs of desirable size in turn their corresponding emission properties. On exposure to UV light, these GQDs emit a variety of rainbow colours depending upon their size and excitation wavelength. This also provides a way for the preparation of either water-soluble or non-polar solvents-soluble GQDs. Most commonly top-down and bottom-up approaches are employed for the synthesis of GQDs and each method has its own advantages and disadvantages. But widely top-down approach is used for the synthesis of large quantity of GQDs [19]. Usually, this method results in GQDs having a large number of surface defects and surface functional groups such as carboxylic acids, epoxy and hydroxyl groups that could further be utilized for functionalization of desired compounds for tailor-made applications [13]. Tetsuka et al. showed tuning of optical properties of GQDs with amine functionalization [7] while Shen et al. demonstrated the surface passivation of GQDs using polyethylene glycol [13]. Sun et al. proposed a sensor for copper ion using modified GQDs [20]. Razmi et al. demonstrated a glucose biosensor using glucose oxidase (GOx) enzyme functionalized GQDs [21]. Liu et al. proposed a selective fluorescent probe to detect and estimate ATP level in cell lysates and in human serum by chemically modifying GQDs with glutathione [5].

Hydrogen peroxide (H_2O_2) plays a vital role in many different fields like biological, clinical, environmental, pharmaceutical and food industries. Moreover, it is also a very important species in biology and biochemical reactions. For example, a higher concentration of H_2O_2 contributes to the oxidative damage of many different enzymes and proteins leading to atrocious effects in human health, and in some cases it may even lead to cancer [22–26]. In the context of chemistry, it is a main by-product in catalytic reactions of *oxidase* enzymes [27, 28]. So, it is very important not only to sense and detect H_2O_2 but also to determine its exact concentration. Basically there are several methods such as spectrophotometry [29], titration methods [30], luminescent techniques [31] and electrochemical methods [32–36] for the detection and quantification of H_2O_2 that have been reported in literature. Among these methods, electrochemical techniques offer simplicity, selectivity, a fast response time for the sensors and involve a less laborious work. Usually, these methods employ enzymes for the detection because of its specificity and effective binding towards a particular analyte [32, 33]. Several strategies involving physical adsorption [34], sol–gel methods [35] and covalent binding [36] are explored for the immobilization of enzymes onto the electrode surface.

Keeping this in mind, in this work we demonstrated a simple strategy to detect and quantify H_2O_2 using electrochemical methods by employing new materials based on *horseradish peroxidase* (HRP) immobilized green colour emitting GQDs (Scheme 1). GQDs of uniform size and shape are prepared using a simple acid reflux of graphite oxide, and on illuminating with UV light, these GQDs emit in the visible region a green colour. Spectroscopic (FTIR, UV–vis, photoluminescence (PL)) and microscopic (transmission electron microscopy, TEM) techniques are used for their structural and morphological characterizations. IR studies reveal the presence of various functional groups namely, hydroxyl, carboxyl and some epoxide groups on GQDs that are being further utilized for HRP immobilization using a simple peptide coupling reaction. Electrochemical techniques namely cyclic voltammetry (CV) and chronoamperometry (CA) are used to demonstrate the enzymatic activity of HRP towards H_2O_2 detection. Several kinetic parameters such as sensitivity, detection limit, linear concentration range and response time are determined for this electrochemical biosensor. Our studies reveal a good electrochemical activity in terms of direct electron transfer of HRP enzyme towards H_2O_2 sensing along with an excellent biocompatibility.

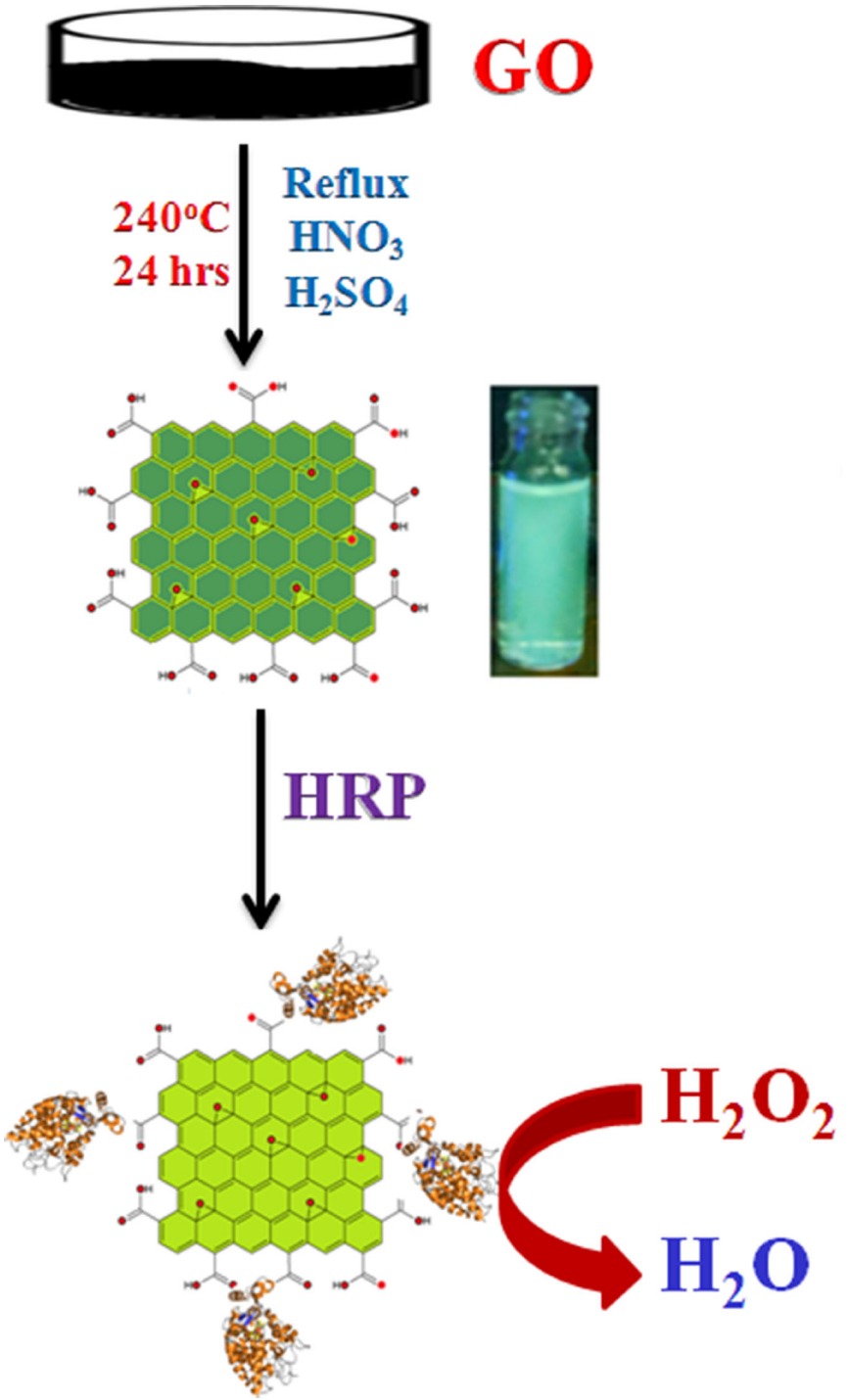

Scheme 1 Schematic representation of the preparation of GQDs and their functionalization with HRP for electrochemical detection of H_2O_2

Materials and Methods

Chemicals

Peroxidase from horseradish as a type VI lyophilized powder (HRP) was obtained from Sigma-Aldrich. Graphite powder, N-hydroxysuccinimide (NHS) and 1-ethyl-3-(3-dimethylaminopropyl)carbodiimide hydrochloride (EDC) were also purchased from Sigma-Aldrich. All other chemicals including sulphuric acid, nitric acid, etc. were procured from Merck and they were used as such without further purification. Millipore water having a resistivity of 18.2 MΩ cm obtained from a quartz distillation unit was used for all the experiments and analysis.

Preparation of Graphene Quantum Dots

GQDs were prepared from graphite oxide using a simple acid reflux method. Initially, graphite oxide was synthesized using a modified Hummers method by the chemical oxidation of graphite powder [4]. About 5 mg of as-prepared graphite oxide was dissolved into 8 ml of HNO_3 and 2 ml of H_2SO_4. To this mixture, 20 ml of millipore water was carefully added and the resulting solution was refluxed at 240 °C for about 24 h by using an oil bath. Then the resulting brown coloured solution was sonicated for about 15 min. Further, the same solution was subjected to filtration using 250 nm microporous and the filtrate was collected separately. Basically, the filtrate is acidic in nature and pH was adjusted to 7.0 using a mild alkali solution in order to obtain a neutral solution. Finally, this solution was purified further using dialysis by employing a dialysis membrane of molecular weight 24,000 Da. The resultant solution is fluorescent in nature, and on illumination with UV light, it emits a green colour. Structural and morphological characterizations of GQDs were performed using spectroscopic (FTIR, UV–vis and PL) and microscopic (TEM) techniques.

Immobilization of *Horseradish Peroxidase* on GQDs

Above-synthesized GQDs were further functionalized with an enzyme, namely HRP. To 5 ml of GQDs, 25 mM EDC and 30 mM NHS were added and the mixture was stirred for 1 h to activate the surface functional groups present in GQDs. About 5 mg of HRP was dissolved in 1 ml of phosphate (PBS) buffer and this solution was added to the above reaction mixture. The resultant solution was stirred at 4 °C for about 12 h to chemically anchor HRP on GQDs using a simple peptide coupling reaction to form an amide linkage. Further, the immobilization of HRP on GQDs was confirmed by using spectroscopic and electrochemical techniques.

Electrochemical Characterization and Biosensor Electrode Preparation

A three-electrode setup was used for the electrochemical characterization. Electrochemical techniques namely CV and CA were used for the analysis. A Pt wire and Ag/AgCl electrode were used as a counter and reference electrodes, respectively. Glassy carbon (GC) electrode was employed as a working electrode. Prior to analysis, the counter electrode Pt wire is cleaned by dipping in concentrated HNO_3 for about 2 min and the reference electrode was thoroughly washed with millipore water. Further, GC electrode was initially polished with a slurry consisting of 0.05 μm alumina powder, followed by cleaning in water and ultrasonication in millipore water for about 15 min. After the pre-cleaning procedure, GC electrode was analysed by recording CV for a well-known redox system namely potassium ferro/ferri cyanide in order

to make sure that the electrode is cleaned properly. Finally, GC was modified with HRP-anchored GQDs by using a simple drop casting method followed by dipping in a chitosan solution for about 1 h and dried under N_2 for a few minutes. Chitosan is basically a bio-compatible polymer and it was used as a binder here to prevent leaching of HRP enzyme from the electrode surface [37, 38]. CV was recorded in an aqueous solution of phosphate buffer (PBS) of pH 7.0 within a potential range from −0.8 to 0.1 V at a sweep rate of 50 mV/s under N_2 atmosphere. Initially, the redox behaviour of HRP enzyme was investigated and then scan rate dependence on the redox peak was also analysed by varying the scan rate from 10 to 100 mV/s. Enzymatic kinetics was studied using CV and CA techniques. CV experiments were carried out in an aqueous phosphate (PBS) buffer solution under N_2 atmosphere at a fixed scan rate of 50 mV/s for incremental additions of hydrogen peroxide (H_2O_2) over a potential ranging from 0.6 to −1.0 V. The concentration of H_2O_2 was varied from 100 μM to 2.66 mM by preparing a stock solution of 10 mM concentration with an incremental addition of 100 μl. CA studies were performed by monitoring H_2O_2 reduction process at a fixed potential of −0.445 V (at which the maximum turnover of HRP enzymatic process occurs), by measuring the corresponding current for each and every additions of H_2O_2. For comparison, similar experiments were also performed using a bare GC electrode and GC electrode modified with GQDs alone without HRP. Several kinetic parameters associated with the enzymatic reaction of H_2O_2 reduction such as sensitivity, limit of detection, linear concentration range and response time were determined. Reproducibility of these electrodes was analysed by repeating the experiments thrice and the values reported were the average value of three measurements. Similarly stability of the enzyme modified electrodes was investigated by studying the enzymatic kinetics over intermittent periods for more than 3 months and analysed the data for its concordance. These enzyme-modified electrodes were stored at 4 °C, whenever it is not in use. These experiments were carried out at room temperature of 25 °C.

Instrumentation

Electrochemical studies were performed using AUTOLAB equipment procured from The Netherlands. The corresponding experiments and their analysis were carried out using General Purpose Electrochemical Software (GPES) provided them. In addition, a few experiments were also performed in Electrochemical Impedance Analyzer, model 6310, EG&G instrument obtained from Princeton Applied Research, USA, and *echem* software provided by them was used for the data collection and analysis. All the other parameters were shown in the respective diagram. Absorbance and fluorescence spectra were recorded using UV–vis PerkinElmer Lamda 650 with Infinite M200MPC model and these spectra were recorded over a wavelength range of 250 to 800 nm. TEM images were analysed using TECNAI G^2 20 FEI model operated at 200 kW. TEM samples were prepared by drop casting method on a copper grid. FTIR spectrum was recorded using Bruker Optic GmbH TENSUR 27 model operated with a software Opus version 6.5 m.

Results and Discussion

Spectroscopic and Microscopic Characterization of GQDs

GQDs prepared by using a simple acid reflux method are characterized using spectroscopic techniques such as UV–vis, fluorescence and FTIR spectroscopy. Further, structural and morphological characterization was performed using TEM. Figure 1A shows the UV–vis

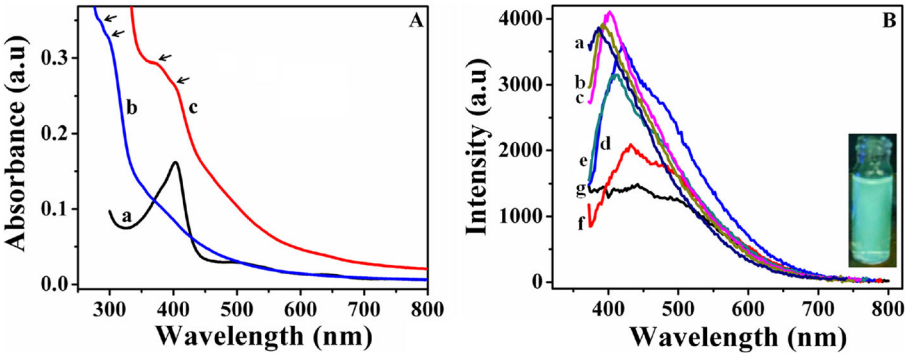

Fig. 1 **A** UV–Vis spectra of free HRP enzyme in aqueous phosphate buffer solution (*a*), GQDs prepared by a simple acid reflux method (*b*) and their functionalization with HRP using a peptide coupling reaction (*c*), respectively. *Arrows* in this figure indicate the position of absorption at which the formation of small peaks and kinks occurs. **B** Photoluminescence (PL) emission spectra of GQDs at various excitation wavelengths viz. (*a*) 330 nm, (*b*) 340 nm, (*c*) 350 nm, (*d*) 360 nm, (*e*) 370 nm, (*f*) 380 nm and (*g*) 390 nm, respectively. *Inset* shows the photograph of GQDs that emit green colour upon UV exposure

spectra of GQDs (b) and HRP immobilized GQDs (c). For comparison, a similar spectrum of HRP in aqueous phosphate buffer solution (a) is also shown. In this figure, the formation of tiny peaks and kinks is denoted by arrows. It can be seen from this figure that GQDs (Fig. 1A (b)) exhibit small peaks as absorption bands at 283 and 298 nm corresponding to $\pi-\pi^*$ and $n-\pi^*$ transitions in addition to a tiny kink at 350 nm. Upon exposure under hand-held UV lamp, these GQDs display an intense green colour and the corresponding fluorescence spectra for various excitation wavelengths (330–390 nm; Fig. 1B (a–g)) are shown in Fig. 1B. It is evident from these PL spectra that GQDs show excitation wavelength-dependent emission spectra and the maximum emission is observed at 350 nm (Fig. 1B (c)) and this wavelength is identified to be an optimal excitation wavelength. This excitation-dependent PL behaviour is quiet common in fluorescent carbon-based materials and is mainly attributed to surface defects, presence of functional groups on the edges and multiphoton active process [13, 39, 40]. On functionalization with an enzyme, HRP, these GQDs show a clear peak at 403 nm corresponding to the Soret absorption band of HRP (Fig. 1A (c)) in addition to absorption peaks of GQDs. For comparison, UV–vis spectrum of free HRP in aqueous phosphate buffer solution is also shown in Fig. 1A (a), which displays a Soret absorption band at 403 nm [27, 28]. Upon functionalization with HRP enzyme, the fluorescence intensity of GQDs is found to be increased. In order to understand the mechanism behind this fluorescence enhancement, PL behaviour of GQDs was investigated before and after functionalization with HRP. Basically, the fluorescence property of GQDs originates from two different types of emissions namely defect state emission (surface energy traps) and intrinsic state emission (electron–hole recombination, quantum size effect) [41, 42]. Initial fluorescence behaviour of GQDs before functionalization arises mainly from the defect state emission. On functionalizing with HRP, several functional groups such as $-OH$ and $-NH_2$ groups are introduced on the surface of GQDs which suppress the defect state emission induced by the initial epoxy and carboxyl groups present on GQDs before functionalization. On the other hand, these electron donor groups introduced via the enzyme immobilization process enhance the integrity of π-conjugated system thereby reducing the surface defects [41, 42]. Consequently, the intensity associated with the intrinsic state emission is increased by facilitating the irradiative recombination of electron–hole pair leading to enhancement in the fluorescence intensity after the enzyme immobilization on GQDs.

Furthermore, mass spectroscopy analysis of HRP-functionalized GQDs showed a maximum intense peak at *m/z* value of 616.4 in addition to several other minor peaks. This high intense peak corresponds to the presence of heme (iron [Fe] containing porphyrin compound with a molecular weight of 616) within the structure of HRP enzyme and the formation of other minor peaks suggests the possibility of various other combination of fragmentation of enzymes which are difficult to analyze. These results clearly confirm the presence of HRP on GQDs and also indicate that HRP retained its native structure without de-naturation after functionalization.

Figure 2A shows the FTIR spectra of GQDs before and after functionalization with HRP enzyme (b and c) along with a free HRP in aqueous phosphate buffer solution (a). As-prepared GQDs before functionalization (Fig. 2A (b)) displayed formation of peaks at 3435 cm^{-1} corresponding to stretching vibration of C–OH groups, 2,923 and 2,853 cm^{-1} corresponding to stretching vibrations of C–H groups, 1,125 and 1,383 cm^{-1} corresponding to carbonyl group and amide III bond, respectively. This particular amide III mode may arise from the combination of N−H bending and stretching vibrations of C–H and C−C groups present on the surface of GQDs. In addition, the vibrational absorption band of C = O at 1,638 cm^{-1} and the epoxide band at 1,112 cm^{-1} are also noted (Fig. 2A (b)). These results confirm the formation of GQDs with various functional groups on its surface. Further, upon immobilizing HRP on these GQDs using a peptide coupling reaction (Fig. 2A (c)), new peaks are formed at 3,145 cm^{-1} representing the stretching vibration of N–H groups and at 1,681 cm^{-1} denoting stretching vibration of C = O groups suggesting the amide bond formation during the functionalization of HRP, in addition to the peaks corresponding to GQDs. For comparison, FTIR spectra of free HRP (Fig. 2A (a)) in aqueous phosphate buffer solution is also shown in Fig. 2A and this shows a broad absorption band at 3,420 cm^{-1} indicating the presence of –OH groups. Further, the morphology and structure of GQDs are analysed by using TEM studies. Figure 2B shows TEM image of GQDs and its corresponding particle size distribution curve is shown in Fig. 2C. It can be seen that GQDs are mono-dispersed, homogenously distributed and uniform in size and shape. These particles are essentially spherical in shape. The average particle size is calculated

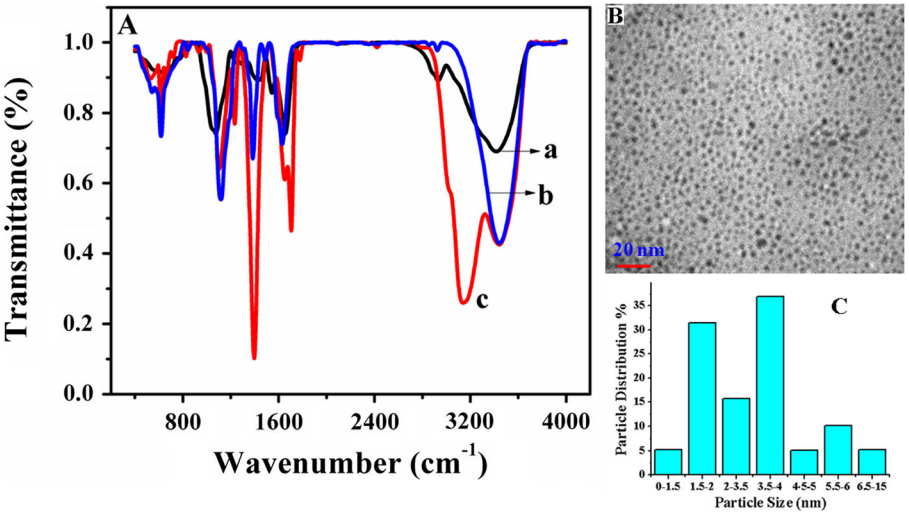

Fig. 2 **A** FTIR spectra of free HRP enzyme in aqueous phosphate buffer solution (*a*), GQDs prepared by a simple acid reflux method (*b*) and their functionalization with HRP using a peptide coupling reaction (*c*), respectively. **B** Transmission electron microscopy (TEM) image of GQDs. *Scale bar* corresponds to 20 nm. **C** Particle size distribution curve obtained from TEM image of GQDs shown in **B**

to be 1.5–4.0±0.3 nm using the particle size distribution curve. Dynamic light scattering (DLS) experiments were also carried out to analyse the particle size distribution of GQDs. These studies reveal the average particle size of GQDs varies between 15 and 20±0.8 nm. The difference in sizes between these two measurements arises because of the phenomena and mechanism involved in the respective experiments [43]. Usually, DLS studies show a higher value since it also taken into account the hydration dynamics of the resultant particles. Nevertheless, these studies clearly suggest the preparation of fluorescent GQDs that emit green colour on exposure to UV light which could further be functionalized with HRP using a peptide bond formation, which is confirmed by spectroscopic and microscopic techniques.

Electrochemical Characterization of HRP Functionalized GQDs

Electrochemical behaviour in terms of redox property and electron transfer process of these HRP-functionalized GQDs is further investigated using CV. HRP-functionalized GQDs were immobilized onto GC electrodes by a simple drop casting method followed by dipping in chitosan binder solution for about 1 h in order to tightly hold the enzyme and to prevent leaching out from the electrode surface [37, 38]. CV studies were performed in an aqueous phosphate buffer solution at a scan rate of 50 mV/s within a potential range from −0.8 to 0.1 V vs. Ag/AgCl. Formation of peaks in CV corresponding to iron redox couple presents within HRP enzyme suggests the direct electron transfer process in the case of HRP-functionalized GQDs. This is particularly significant because the electron transfer process occurs for HRP-functionalized GQDs without the addition of any external redox mediators. The enzyme peroxidase is an oxidoreductase enzyme containing a heme cofactor in its active site. The redox activity of its active site is due to Fe(III)/Fe(II) electron transfer reaction. The formal potential of this redox process is determined to be −0.323 V which is very close to −0.22 V, the formal potential of HRP in its native structure [44]. A small difference in the potential value may arise from the structural arrangement, orientation and accessibility of the redox groups present within HRP on these GQDs surface. The observed redox response in our case is attributed to Fe(III)/Fe(II) species associated with the heme groups of the HRP enzyme. Moreover, the effect of scan rate on the redox behaviour of HRP was investigated over a wide range of sweep rate from 10 to 100 mV/s. The corresponding cyclic voltammograms were displayed in Fig. 2A (a–j). It can be seen that the redox current increases systematically with the increase in scan rate with a minor shift in redox potential values. It is also worth mentioning here that the formation of reverse peak (reduction) is very clear compared to the forward oxidation peak. This is attributed to the fact that the active centre, a heme cofactor of HRP, is deeply buried within the protein matrix of HRP enzyme and the redox peak will usually be formed depending upon the orientation and access to the redox centre along with the electron transfer rate constants associated with that processes. In addition, the scan rate used for the studies is also vital to clearly see the redox peaks. In our case, the oxidation peak is not clear because of the poor electron transfer corresponding to oxidation process of the redox centre owing to its improper orientation [27, 28, 44] and it is worth mentioning here that this peak is slightly visible at higher scan rate suggesting the probable higher rate constant value for the oxidation process. But the reduction peak is very clear and the reduction current increases systematically with the rise in scan rate. Figure 3B displays the plot of peak current corresponding to both the oxidation (a) and reduction (b) processes with respect to square root of scan rate. It can be noted that I_p vs. $\nu^{1/2}$ plots show a linear relation, indicating that the electron transfer process is diffusion controlled. This also suggest that HRP is surface confined, immobilized onto GC electrodes through GQDs and retains its redox property, involved in direct electron transfer process and does not undergo any structural deformation while

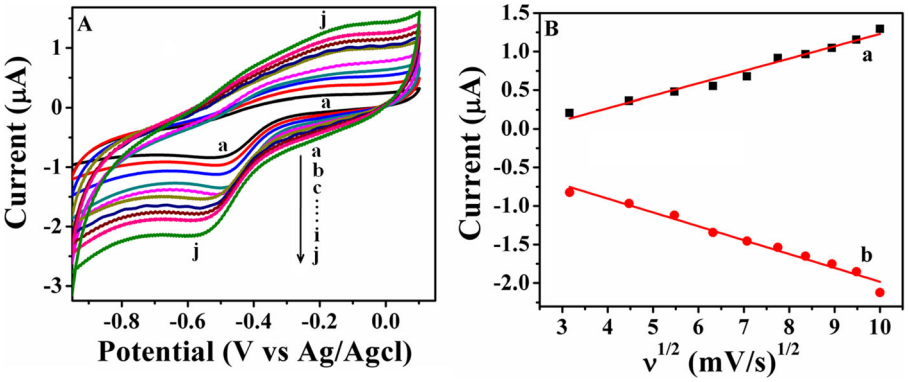

Fig. 3 **A** Cyclic voltammograms of HRP-functionalized GQDs immobilized onto GC electrode in phosphate buffer aqueous solution (pH=7.0) showing the effect of scan rate. CVs were recorded at different scan rates namely (*a*) 10 mV/s, (*b*) 20 mV/s, (*c*) 30 mV/s, (*d*) 40 mV/s, (*e*) 50 mV/s, (*f*) 60 mV/s, (*g*) 70 mV/s, (*h*) 80 mV/s, (*i*) 90 mV/s and (*j*) 100 mV/s, respectively. **B** Current vs. $\nu^{1/2}$ plots of HRP-functionalized GQDs immobilized onto GC electrode for both the oxidation (*a*) and reduction (*b*) processes. These data points were collected from the corresponding CVs shown in **A**

potential cycling. This also supports our observation from spectroscopic characterization that HRP has been functionalized on GQDs and retains its structure and activity.

Electrochemical Biosensor for Hydrogen Peroxide

HRP-functionalized GQDs were further explored for the possibility of fabrication of an electrochemical biosensor for H_2O_2 detection. These studies were carried out by monitoring the enzymatic activity corresponding to reduction of H_2O_2 in aqueous phosphate buffer solution using CV and CA techniques. Generally, colorimetric techniques are employed for H_2O_2 detection using GQDs without HRP enzyme [45], which is primarily non-selective, required additional reagents that are toxic and harmful and user dependent. In this work, an enzymatic detection is employed, by using HRP-functionalized GQDs immobilized onto GC electrode. This particular electrochemical biosensor is very selective and direct electron transfer process is involved in the reduction of H_2O_2 that can be monitored easily using electrochemical techniques such as CV and CA. Figure 4A shows the CVs of HRP-functionalized GQDs electrodes towards the addition of various concentrations of H_2O_2 (Fig. 4A (b–k)) in aqueous phosphate buffer solution (pH=7.0) under N_2 atmosphere at a scan rate of 50 mV/s. For comparison, CV of HRP-immobilized GQDs electrode (under similar conditions) before the addition of H_2O_2 is also shown in Fig. 4A (a). It can be seen that the enzyme modified electrode displayed a redox peak corresponding to Fe(III)/Fe(II) redox reaction of heme groups present within the enzyme. Upon addition of H_2O_2, a significant enhancement in the reduction current was observed. A systematic increase in H_2O_2 concen tration results in systematic increase of the reduction current. On adding 100 μM H_2O_2, a threefold enhancement in the reduction current (Fig. 4A (b)) was observed. A wide concentration of H_2O_2 ranging from 100 μM to 2.66 mM was used for the study and for clarity CVs representing 100 μM to 1 mM (Fig. 4A (b–k)) concentrations of H_2O_2 were shown in Fig. 4A. A plot of reduction current vs. concentration is displayed in Fig. 4B. A linear variation of reduction current with increasing concentration of H_2O_2 is noted. The onset potential of H_2O_2 reduction is determined to be −0.32 V, which is exactly the formal potential of HRP enzyme indicating the involvement of enzyme in the reduction process. The half-wave potential for

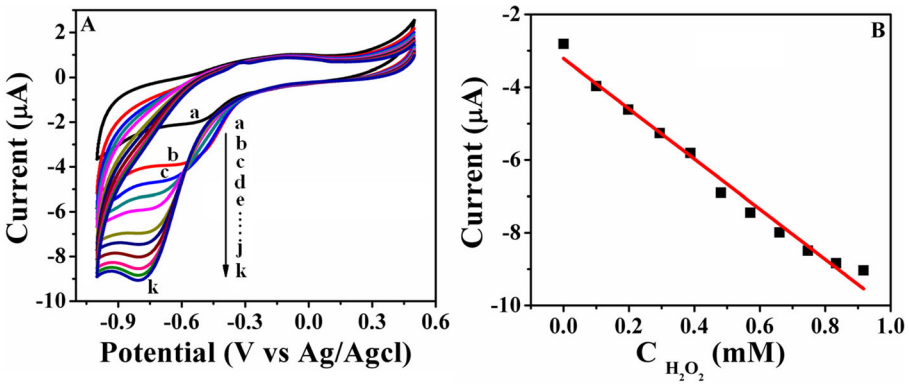

Fig. 4 **A** Cyclic voltammograms corresponding to HRP-functionalized GQDs immobilized onto GC electrode in aqueous phosphate buffer solution (pH=7.0) at a fixed sweep rate of 50 mV/s showing the bio-electrocatalytic response towards the addition of various concentrations of H_2O_2 such as (*a*) 0 μM, (*b*) 100 μM, (*c*) 198 μM, (*d*) 294 μM, (*e*) 388 μM, (*f*) 481 μM, (*g*) 571 μM, (*h*) 660 μM, (*i*) 747 μM, (*j*) 833 μM and (*k*) 917 μM, respectively. For comparison CV of a similar electrode before the addition of H_2O_2 is also shown as *a*. In this figure, *arrow* indicates the direction of increasing concentration of H_2O_2. **B** A plot of current vs. concentration for various additions of H_2O_2. Data points were collected from CV measurements shown in **A**

H_2O_2 reduction was determined to be −0.445 V. This significant increase in the reduction current suggests the bioelectrocatalytic activity of HRP enzyme, where a fast direct electron transfer between the electrode and heme groups of the immobilized enzyme occurs because of the favorable orientation and accessibility of redox groups present within the HRP enzyme. Similar experiments of HRP enzyme-based H_2O_2 reduction without GQDs are also performed and in that case no significant increase in the reduction current was observed. These results clearly indicate the facilitation of direct electron transfer of HRP using GQDs in H_2O_2 sensing experiments.

Amperometric Study of H_2O_2 Biosensor

CV results described above indicate the possibility of determining H_2O_2 concentration by fabricating an amperometric biosensor based on HRP-functionalized GQDs. In the case of HRP immobilized on GQDs-coated electrodes, turnover of the enzyme occurs at −0.445 V vs. Ag/AgCl and for the amperometric studies this potential was selected for the detection of H_2O_2. Figure 5A shows a typical current vs. time plots for bare GC electrode (a), GQDs-modified GC electrode in absence of HRP (b) and HRP-functionalized GQDs electrode (c) obtained by successive addition of small amounts of H_2O_2 to a continuously stirred aqueous phosphate buffer solution (pH=7.0). CA experiments were performed by monitoring the change in reduction current after attaining the steady state at a fixed potential of −0.445 V for each and every additions of H_2O_2. In our studies, we find that the steady state reduction current reached within 10 s after the addition. Enlarged view of the same plot for the initial time period was shown as inset in Fig. 5A. It can be noted that each incremental addition of H_2O_2 results in increase of its reduction current. Compared to bare GC and GQDs without HRP, the enzyme-modified electrodes showed a dramatic increase in the reduction current. Typical staircase model response is obtained for the incremental addition of H_2O_2. Response time of this particular electrochemical biosensor is very rapid and it is determined to be within 2–3 s. Although initial change in the reduction current corresponding to H_2O_2 addition seems to be very small, HRP-functionalized GQDs modified GC electrode displayed a remarkable

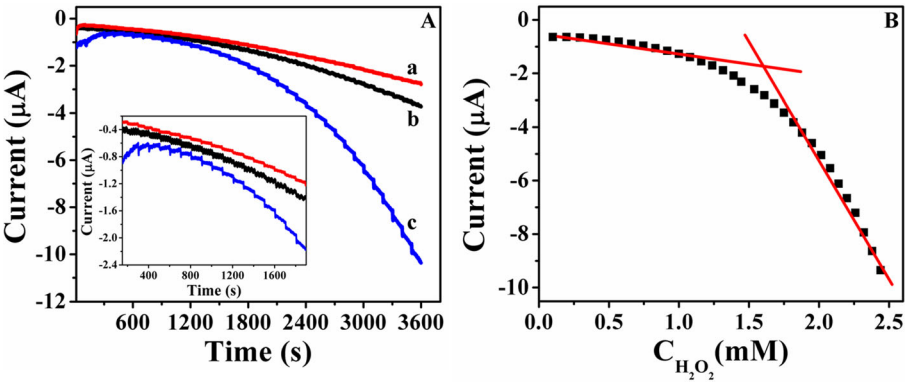

Fig. 5 **A** Chronoamperometric graphs of bare GC electrode (*a*), GQDs-immobilized GC electrode (*b*) and HRP-functionalized GQDs anchored onto GC electrode (*c*) for incremental additions of H_2O_2. The concentration of H_2O_2 was varied from 100 μM to 2.66 mM. *Inset* shows the enlarged view of the same graphs during initial time period. **B** Calibration curve of current vs. concentration of H_2O_2 and the corresponding data points were collected from chronoamperometric plots shown in **A**

change in the reduction current for higher concentrations when compared to other electrodes analysed in this work. The change in reduction current is estimated to be four and six times higher for HRP-functionalized GQDs in comparison to GQDs without HRP and bare GC electrodes, respectively. These results clearly reveal a quick and fast response for H_2O_2 sensor along with a high sensitivity. Fig. 5B display a plot of reduction current vs. concentration of H_2O_2 for HRP-functionalized GQDs modified electrode. It can be seen from this plot that each incremental addition of H_2O_2 results in increase of its corresponding reduction current and a linear variation with respect to concentration is noted. Using these data, the sensitivity and detection limit values are calculated based on the following formulae,

$$\text{Sensitivity}\ \ (\sigma) = \sqrt{\text{Sum}\left(I - \bar{\text{I}}\right)^2 / n} \tag{1}$$

$$\text{Detection}\ \ \text{limit} = 3\sigma / \ \text{slope} \tag{2}$$

Where σ is sensitivity of the electrode, I is the current measured due to addition of increasing concentration of H_2O_2, $\overline{I}$ is the average current change, n is the number additions carried out for H_2O_2 sensing experiment and slope denotes the slope of current vs. concentration plot, respectively. It is evident from this plot that there are two linear regions for H_2O_2 detection. The first linear region is from 100 μM to 1.3 mM and the second linear region is from 1.7 to 2.6 mM. With respect to these two linear regions and by using Eqs. (1) and (2), both the sensitivity and limit of detection values were calculated. Sensitivity values of 0.905 and 7.057 μA/mM for the respective first and second linear regions are determined for this electrochemical biosensor. Similarly, the detection limit values are found to be 530.85 nM and 2.16 μM, respectively. In the case of bare GC electrode and GQDs without HRP-modified GC electrode, the sensitivity values are estimated to be 0.856 and 112 nA/mM, respectively. These values are very much lower compared to the sensitivity value obtained for HRP-functionalized GQDs electrode. On comparison, sensitivity values are almost 3 orders of magnitude higher for HRP-functionalized GQDs-coated GC electrode. The main reason for this behaviour is attributed to the enhancement in enzyme loading and its reaction with the aid of facilitated

direct electron transfer through GQDs along with the favourable orientation of HRP on these electrodes. The sensitivity, limit of detection and linear concentration range values reported in this work are an average value of three repeated measurements. We observed a very small deviation of ~2 % change in the reduction current values for the repeated electrochemical response analysis. The proposed electrochemical, enzymatic H_2O_2 sensor is found to be quite stable for more than 3 months and even at the end of 3 months the hydrogen peroxide reduction current is observed to be decreased by 97 % of its original value. These HRP-functionalized GQDs modified GC electrodes are stored at 4 °C when not in use. Remarkably, this particular electrochemical biosensor is found to be stable and reversible for at least 90 days.

The estimated kinetic parameters such as the sensitivity, detection limit and linear concentration range values are compared with some of the other reported values for H_2O_2 sensor in the literature and the comparison is shown in Table 1 [44, 46–56]. It can be noted that the proposed sensor yielded a higher sensitivity and a wide linear range of detection for H_2O_2 sensor when compared to other sensors while the limit of detection is almost comparable with that of the other reports [37, 38, 53, 55, 56]. Moreover, some of the H_2O_2 sensors reported require a redox mediator for the detection purpose, which is not a critical factor in this sensor as it involves a direct electron transfer process for the reduction of H_2O_2 facilitated further by the presence of GQDs. Observance of two linear regions for H_2O_2 sensor reported in this work is pretty unusual and surprising. It is mainly attributed to the sensing components and arrangement in terms of orientation of enzymes along with the fabrication method adapted. Careful analysis of these regions suggests that the first linear region arises from the loosely bound enzymes and the direct access of H_2O_2 to the electrode surface through pinholes and defects; in this case, the change in H_2O_2 reduction current is very minimal. On the other hand, the relative change in reduction current for each addition of H_2O_2 is quite significant and higher in the second region where the chemically bound enzymes through functionalization plays a major role in H_2O_2 detection. The main reason for this behaviour is due to enhancement in the enzymatic reaction with the aid of facilitated electron transfer through GQDs and favourable orientation of HRP on GQDs.

Table 1 Comparison of kinetic parameters such as sensitivity, linear concentration range and detection limit for the proposed H_2O_2 biosensor based on HRP-functionalized GQDs immobilized onto GC electrode with the other electrode materials reported for enzymatic H_2O_2 detection

S. no.	Electrode material	Sensitivity	Linear concentration range	Detection limit	Reference
1.	ERGO/HRP	0.090 μA/mM	9–195 μM	9 μM	[38]
2.	Au–GS/HRP/CS	–	5 μM–5.13 mM	1.7 μM	[37]
3.	PANI/HRP/Graphene–CNT/Nafion/AuPt	37 mA/mM	0.5 μM–0.1 mM	0.17 μM	[56]
4.	Nafion/HRP/Graphene/GC	0.11 μA/mM	0.33–13.0 μM	100 nM	[57]
5.	HRP/GO/Nafion/GC	–	1.0 μM–1.0 mM	0.40 μM	[58]
6.	HRP/Au NP/GC	0.25 mA/mM	6.1 μM–1.8 mM	6.1 μM	[59]
7.	HRP/PAMAM/GC	0.36 mA/mM	3.1 μM–2.0 mM	0.8 μM	[60]
8.	HRP/PANI/GC	–	1.0 μM–2.0 mM	0.6 μM	[61]
9.	HRP/GQDs/GC	0.905 and 7.057 μA/mM	100 μM–1.3 mM and 1.7–2.6 mM	530.85 nM and 2.16 μM	This work

ERGO electrochemically reduced graphene oxide, *HRP* horseradish peroxidase, *GQDs* graphene quantum dots, *Au–GS* gold decorated graphene sheets, *CS* chitosan, *PANI* polyaniline, *CNT* carbon nanotubes, *GC* glassy carbon electrode, *GO* graphene oxide, *NP* nanoparticles, *PAMAM* poly(amidoamine) dendrimers

Nevertheless, a successful fabrication of H_2O_2 electrochemical biosensor based on HRP-immobilized GQDs is demonstrated.

Mechanism of H_2O_2 Sensing

Based on the above experimental results and observation, a simple mechanism is proposed for the enzymatic detection of H_2O_2 using HRP-functionalized GQDs. Basically, the enzyme *horseradish peroxidase* consists of a heme prosthetic group as its active redox centre with iron having an oxidation state of Fe(III). In presence of H_2O_2, Fe(III) present within HRP-immobilized biosensor surface is oxidized to form an intermediate compound I. The possible catalytic mechanism of HRP towards H_2O_2 reduction can be expressed as follows:

$$\mathrm{HRP}\left(\mathrm{Fe}^{3+}\right) + \mathrm{H_2O_2} \rightarrow \mathrm{Compound\ I}\left(\mathrm{Fe}^{4+} - \mathrm{O}\right) + \mathrm{H_2O} \tag{3}$$

$$\mathrm{Compound\ I}\ \left(\mathrm{Fe}^{4+} - \mathrm{O}\right) + \mathrm{e}^{-} + \mathrm{H}^{+} \rightarrow \mathrm{Compound\ II} \tag{4}$$

$$\mathrm{Compound\ II} + \mathrm{e}^{-} + \mathrm{H}^{+} \rightarrow \mathrm{HRP}\left(\mathrm{Fe}^{3+}\right) + \mathrm{H_2O} \tag{5}$$

Compound I is a two equivalent oxidized form containing oxy-ferryl heme (Fe^{+4}–O) and a porphyrin π-cation radical that exhibits a good catalytic activity [57–59]. Porphyrin radical accepts one electron from the electrode surface through GQDs to form a second intermediate, Compound II. Subsequently, this compound is reduced back to the native HRP by accepting one more electron from the electrode with the aid of GQDs [57–59]. Direct adsorption of such proteins and enzymes on the electrode surfaces frequently results in the de-naturation of proteins and loss of their biological activities [60, 61]. In order to avoid such things, in our work HRP enzyme is functionalized on GQDs through a simple coupling reaction between the amine group of enzyme and the acid groups of GQDs leading to a peptide bond formation. Moreover, GQDs also act as a facilitator of direct electron transfer between HRP enzyme and the electrode, which is further explored for the successful fabrication of electrochemical biosensor for H_2O_2 detection.

Conclusions

Mono-disperse, homogeneous and highly uniform spherical particles of fluorescent GQDs which emit green colour on exposure to UV light are successively prepared using a simple acid reflux method. Subsequently, these GQDs are functionalized with HRP and demonstrated these functionalized GQDs as a potential electrochemical biosensor for H_2O_2 detection. Spectroscopic techniques namely FTIR, UV–Vis, PL studies and TEM analysis are used for the characterization of structure and morphology of these GQDs. Electrochemical techniques such as CV and CA are employed to investigate redox property, electron transfer behaviour and H_2O_2 sensing experiments. A good linear range of detection, higher sensitivity, lower detection limit and a fast response time for H_2O_2 detection is obtained using HRP-functionalized GQDs. Overall, in this work, we demonstrated a simple strategy to prepare and functionalize GQDs that could be used further for the fabrication of electrochemical biosensors. Here, HRP is shown as an example and this methodology can easily be extended to other enzymes, proteins and biomolecules.

Acknowledgments The authors acknowledge the funding from Department of Science and Technology (DST), India, and CSIR, India, through Network Projects having the project numbers GAP 16/10 and CSC 0134, respectively, for carrying out this research work. AM is thankful to CSIR for Junior Research Fellowship to pursue Ph.D. program. Central Instrumentation Facility (CIF) of CSIR–CECRI is also acknowledged for providing FTIR and TEM facilities for characterization.

References

1. Brownson, D. A. C., Kampouris, D. K., & Banks, C. E. (2012). *Chemical Society Reviews, 41*, 6944–6976.
2. Chen, D., Feng, H., & Li, J. (2012). *Chemical Reviews, 112*, 6027–6053.
3. Yao, J., Sun, Y., Yang, M., & Duan, Y. (2012). *Journal of Materials Chemistry, 22*, 14313–14329.
4. Hummers, W. S., & Offeman, R. E. (1958). *Journal of the American Chemical Society, 80*, 1339–1339.
5. Liu, J. J., Zhang, X. L., Cong, Z. X., Chen, Z. T., Yang, H. H., & Chen, G. N. (2013). *Nanoscale, 5*, 1810–1815.
6. Jiang, F., Chen, D., Li, R., Wang, Y., Zhang, G., Li, S., Zheng, J., Huang, N., Gu, Y., Wang, C., & Shu, C. (2013). *Nanoscale, 5*, 1137–1142.
7. Tetsuka, H., Asahi, R., Nagoya, A., Okamoto, K., Tajima, I., Ohta, R., & Okamoto, A. (2012). *Advanced Materials, 24*, 5333–5338.
8. Zheng, L., Chi, Y., Dong, Y., Lin, J., & Wang, B. (2009). *Journal of the American Chemical Society, 131*, 4564–4565.
9. Zhu, S., Zhang, J., Qiao, C., Tang, S., Li, Y., Yuan, W., Li, B., Tian, L., Liu, F., Hu, R., Gao, H., Wei, H., Zhang, H., Sun, H., & Yang, B. (2011). *Chemical Communications, 47*, 6858–6860.
10. Liu, R., Wu, D., Liu, S., Koynov, K., Knoll, W., & Li, Q. (2009). *Angewandte Chemie International Edition, 48*, 4598–4601.
11. Pan, D., Guo, L., Zhang, J., Xi, C., Xue, Q., Huang, H., Li, J., Zhang, Z., Yu, W., Chen, Z., Li, Z., & Wu, M. (2012). *Journal of Materials Chemistry, 22*, 3314–3318.
12. Zhang, M., Bai, L., Shang, W., Xie, W., Ma, H., Fu, Y., Fang, D., Sun, H., Fan, L., Han, M., Liu, C., & Yang, S. (2012). *Journal of Materials Chemistry, 22*, 7461–7467.
13. Shen, J., Zhu, Y., Chen, C., Yang, X., & Li, C. (2011). *Chemical Communications, 47*, 2580–2582.
14. Zhuo, S., Shao, M., & Lee, S. T. (2012). *ACS Nano, 6*, 1059–1064.
15. Jing, Y., Zhu, Y., Yang, X., Shen, J., & Li, C. (2010). *Langmuir, 27*, 1175–1180.
16. Liu, Z., Robinson, J. T., Sun, X., & Dai, H. (2008). *Journal of the American Chemical Society, 130*, 10876–10877.
17. Yang, F., Zhao, M., Zheng, B., Xiao, D., Wu, L., & Guo, Y. (2012). *Journal of Materials Chemistry, 22*, 25471–25479.
18. Fan, L., Hu, Y., Wang, X., Zhang, L., Li, F., Han, D., Li, Z., Zhang, Q., Wang, Z., & Niu, L. (2012). *Talanta, 101*, 192–197.
19. Wang, D., Wang, L., Dong, X., Shi, Z., & Jin, J. (2012). *Carbon, 50*, 2147–2154.
20. Sun, H., Gao, N., Wu, L., Ren, J., Wei, W., & Qu, X. (2013). *Chemistry - A European Journal, 19*, 13362–13368.
21. Razmi, H., & Rezaei, R. M. (2013). *Biosensors and Bioelectronics, 41*, 498–504.
22. Li, L. L., Ji, J., Fei, R., Wang, C. Z., Lu, Q., Zhang, J. R., Jiang, L. P., & Zhu, J. J. (2012). *Advanced Functional Materials, 22*, 2971–2979.
23. Ma, L., Yuan, R., Chai, Y., & Chen, S. (2009). *Journal of Molecular Catalysis B: Enzymatic, 56*, 215–220.
24. Wang, H. S., Pan, Q. X., & Wang, G. X. (2005). *Sensors, 5*, 266–276.
25. Chen, S., Yuan, R., Chai, Y., Yin, B., Li, W., & Min, L. (2009). *Electrochimica Acta, 54*, 3039–3046.
26. Zhang, H. L., Lai, G. S., Han, D. Y., & Yu, A. M. (2008). *Analytical and Bioanalytical Chemistry, 390*, 971–977.
27. Thenmozhi, K., & Narayanan, S. S. (2007). *Bioanalytical Chemistry, 387*, 1075–1082.
28. Rejeb, I. B., Arduini, F., Amine, A., Gargouri, M., & Palleschi, G. (2007). *Analytica Chimica Acta, 594*, 1–8.
29. Hua, M. Y., Lin, Y. C., & Tsai, R. Y. (2012). *Journal of Materials Chemistry, 22*, 2566–2574.
30. Xiao, Y., Ju, H. X., & Chen, H. Y. (2000). *Analytical Biochemistry, 278*, 22–28.
31. Wang, G., Xu, J. J., & Chen, H. Y. (2003). *Biosensors and Bioelectronics, 18*, 335–343.
32. Roy, J., Abraham, T. E., Abhijith, K. S., Sujith Kumar, P. V., & Thakur, M. S. (2005). *Biosensors and Bioelectronics, 21*, 206–211.
33. Zhang, Y., Zeng, G. M., Tang, L., Huang, D. L., Jiang, X. Y., & Chen, Y. N. (2007). *Biosensors and Bioelectronics, 22*, 2121–2126.
34. Caramori, S. S., & Fernandes, K. F. (2004). *Process Biochemistry, 39*, 883–888.

35. Won, Y. H., Aboagye, D., Jang, H. S., Jitianu, A., & Stanciu, L. A. (2010). *Journal of Materials Chemistry, 20*, 5030–5034.
36. Chen, H. C., Hua, M. Y., Liu, Y. C., Yang, H. W., & Tsai, R. Y. (2012). *Journal of Materials Chemistry, 22*, 13252–13259.
37. Zhou, K., Zhu, Y., Yang, X., Luo, J., Li, C., & Luan, S. (2010). *Electrochimica Acta, 55*, 3055–3060.
38. Selvakumar, P., Binesh, U., & Chen, S. M. (2012). *International Journal of Electrochemical Science, 7*, 7935–7947.
39. Loh, K. P., Bao, Q., Eda, G., & Chhowalla, M. (2010). *Nature Chemistry, 2*, 1015–1024.
40. Liu, H., Ye, T., & Mao, C. (2007). *Angewandte Chemie International Edition, 446*, 6473–6475.
41. Zhu, S., Zhang, J., Tang, S., Qiao, C., Wang, L., Wang, H., Liu, X., Li, B., Li, Y. F., Yu, W., Wang, X. F., Sun, H. C., & Yang, B. (2012). *Advanced Functional Materials, 22*, 4732–4740.
42. Li, L., Wu, G., Yang, G. H., Peng, J., Zhao, J., & Zhu, J. J. (2013). *Nanoscale, 5*, 4015–4039.
43. Sathish, K. K., Ganesh, V., Palaniappan, A., & Sheela, B. (2014). *Materials Chemistry and Physics, 143*, 1325–1330.
44. Polsky, R., Harper, J. C., Dirk, S. M., Arango, D. C., Wheeler, D. R., & Brozik, S. M. (2007). *Langmuir, 23*, 364–366.
45. Yi, X., Xian, J. H., & Yuan, C. H. (2000). *Analytical Biochemistry, 1*, 22–28.
46. Wang, L., & Wang, E. (2004). *Electrochemistry Communications, 6*, 225–229.
47. Xiang, C., Zou, Y., Sun, L., & Xu, F. (2008). *Analytical Letters, 41*, 2224–2226.
48. Chen, H., & Dong, S. (2007). *Biosensors and Bioelectronics, 22*, 1811–1815.
49. Zhao, X., Mai, Z., Kang, X., & Zou, X. (2008). *Biosensors and Bioelectronics, 23*, 1032–1038.
50. Farzana, S., Ganesh, V., & Berchmans, S. (2013). *Journal of the Electrochemical Society, 160*, H573–H580.
51. Sheng, Q., Wang, M., & Zheng, J. (2010). *Sensors and Actuators B: Chemical, 160*, 1070–1077.
52. Li, M., Xu, S., Tang, M., Liu, L., Gao, F., & Wang, Y. (2011). *Electrochimica Acta, 56*, 1144–1149.
53. Zhang, L., Cheng, H., & Zhang, H. (2012). *Electrochimica Acta, 65*, 122–126.
54. Lei, C. X., Wang, H., Shen, G. L., & Yu, R. Q. (2004). *Electroanalysis, 16*, 736–740.
55. Zeng, Y. L., Huang, H. W., Jiang, J. H., Tian, M. N., & Li, C. X. (2007). *Analytica Chimica Acta, 604*, 170–176.
56. Xua, Q., Zhua, J. J., & Hu, X. Y. (2007). *Analytica Chimica Acta, 597*, 151–156.
57. Gu, B. X., Xu, C. X., Zhu, G. P., Liu, S. Q., Chen, L. Y., Wang, M. L., & Zhu, J. J. (2009). *Journal of Physical Chemistry B, 113*, 6553–6557.
58. Dimcheva, N., & Horozova, E. (2005). *Analytical and Bioanalytical Chemistry, 382*, 1374–1379.
59. Zhao, J., Henkens, R., Stonehuerner, T., O'Daly, J., & Crunbliss, A. (1992). *Journal of Electroanalytical Chemistry, 327*, 109–119.
60. Yang, Y., Yang, G., Huang, Y., Bai, H., & Lu, X. (2009). *Colloids and Surfaces A, 340*, 50–55.
61. Liu, Y., Yuan, R., & Chai, Y. Q. (2006). *Sensors and Actuators B: Chemical, 115*, 109–115.